Engineered Science
DOI: https://dx.doi.org/10.30919/es1308

# Simulation of Thermal Effects on Rectal Wall During Laser Treatment of Prostate Cancer Using Hyaluronic Acid and Polyethylene Glycol (PEG) Spacers: A Generalized Dual-Phase-Lag (GDPL) Bioheat Approach

Phanuwat Boontatao,[1] Nattadon Pannucharoenwong,[1,*] Direk Nualsing,[1,*] Totsaphon Chabuanoi,[1] Phadungsak Rattanadecho,[1] Teeravut Tubtawee[2] and Suphasit Panvichien[3]

## Abstract

Prostate cancer is the most prevalent cancer among men and a leading cause of mortality. Laser radiation therapy is a critical treatment modality, utilizing high heat to ablate prostate tumors and effectively eliminate cancer cells. However, the excessive heat generated during treatment poses a risk of damaging adjacent healthy tissues, particularly the rectal wall. This study presents a method to mitigate thermal effects on the rectal wall by using Hyaluronic Acid (HA) or Polyethylene Glycol (PEG) spacers. These spacers are injected between the rectum and prostate during laser therapy to reduce unintended thermal damage. Thermal effects were analyzed using the Generalized Dual-Phase Lag (GDPL) bioheat equations, comparing the impact of HA and PEG spacers for tumor sizes of 10 mm, 15 mm, and 20 mm. Results demonstrate that HA injection significantly reduces the maximum temperature on the rectal wall compared to cases without a spacer. For tumor sizes of 10 mm, 15 mm, and 20 mm, temperature reductions of 3.0%, 13.2%, and 74.1% were observed, respectively, with HA outperforming PEG. Notably, the laser heat eliminated a 10 mm tumor within 60 seconds. The authors acknowledge the necessity of clinical trials to validate these benefits. While this study has certain limitations, it offers preliminary insights to physicians on the potential advantages of using HA to enhance temperature management during radiation therapy for prostate cancer.

*Keywords:* Prostate cancer; Hyaluronic acid; Polyethylene Glycol; Dual-phase lag; Laser irradiation therapy.
Received: 16 September 2024; Revised: 15 October 2024; Accepted: 31 October 2024.
Article type: Research article.

## 1. Introduction

Prostate cancer is a growing global health concern, with over 1.41 million new cases and 375,304 deaths reported worldwide in 2020. It remains the most commonly diagnosed cancer in men, ranking among the top causes of cancer-related mortality in the United States and Europe. In 2022, more than 18 million Americans with a history of cancer were alive, with prostate cancer affecting approximately 3.52 million men, making it a significant public health issue.[1-2] The disease often leads to complications such as urinary obstruction, which can severely impact the patient's quality of life. While age and family history are well-known risk factors for prostate cancer, other factors such as diet, obesity, smoking, and environmental exposures, including certain occupational hazards like cadmium and ionizing radiation, have also been investigated.[3]

Despite advances in understanding risk factors, prostate cancer management continues to pose challenges, particularly in preserving healthy tissue during treatment. Current treatment options include surgery and radiation therapy; however, studies suggest that these approaches may not significantly reduce mortality compared to active surveillance, especially in low to moderate-risk tumors.[3,4] As a result, there

[1] *Department of Mechanical Engineering, Faculty of Engineering, Thammasat School of Engineering, Thammasat University, Bangkok, 12120, Thailand*
[2] *Department of Radiology, Faculty of Medicine, Prince of Songkla University, Hat Yai, 90110, Thailand*
[3] *School of Biomedical Engineering & Imaging Sciences, Faculty of Life Sciences & Medicine, King's College London, London, WC2R 2LS, United Kingdom*
**Email:* pnattado@engr.tu.ac.th (N. Pannucharoenwong), ndirek@engr.tu.ac.th (D. Nualsing)

has been growing interest in more targeted therapies, such as Focal Laser Ablation (FLA). FLA delivers focused heat energy to the tumor, causing thermal ablation with minimal impact on surrounding structures, including reproductive and urinary functions. Its advantages — compatibility with Magnetic resonance imaging (MRI), lower costs, and faster patient recovery — have made it an attractive option for localized prostate cancer treatment. The effectiveness of laser ablation relies on precise temperature control, with studies indicating that temperatures above 43 °C cause irreversible cellular damage. This damage occurs through multiple mechanisms, including protein denaturation, loss of membrane integrity, and disruption of DNA repair enzymes.[5-7]

In prostate cancer cases, particularly when tumors are located in the peripheral zone near the rectum, laser therapy poses a risk of rectal wall injury, a common side effect of radiation treatments. To mitigate the risk, various rectal spacers—such as hyaluronic acid (HA), polyethylene glycol (PEG), collagen, and saline-filled balloon implants—have been used to create physical separation between the rectum and prostate. An ideal spacer should possess tissue-equivalent properties to avoid interference with radiation dose distribution, be biocompatible, and maintain its shape throughout the duration of treatment.[8-10]

In prostate cancer treatment, the use of spacers in the perirectal tissue helps reduce gastrointestinal side effects. In medical practice, PEG hydrogel must be injected relatively quickly due to its rapid solidification, unlike HA, which allows for a slower, more controlled injection. However, HA spacers are more viscous and tend to form cohesive clumps more effectively than PEG. HA has gained wide acceptance in medical applications due to its excellent biocompatibility, biodegradability, and structural properties. HA hydrogels, derived from natural polymers, are known for their flexibility and ability to retain water, making them ideal for mimicking physiological tissue.[11] Conversely, PEG hydrogels, though similarly biocompatible, offer different mechanical properties and have been shown to significantly reduce rectal radiation exposure in clinical applications.[12-14]

This study is the first to employ a numerical model to analyze the thermal behavior of using HA as a rectal spacer in laser therapy for prostate cancer. By incorporating the complex structure of biological tissues and their vascular networks, this research introduces an innovative method for evaluating thermal effects during treatment. The study uses the Generalized Dual-Phase Lag heat transfer model to address temperature, and heat flux phase lags, addressing the thermal responses of porous tissues during laser irradiation. This approach provides a novel perspective on hyperthermia in prostate cancer treatment, with a focus on how vascular networks influence the thermal parameters during laser ablation.[15]

This research focuses on modeling the thermal protective effects of HA and PEG spacers placed between the rectal wall and prostate tumor under laser treatment. These spacers aim to reduce the heat-induced damage to surrounding rectal tissues throughout laser ablation. The study evaluates thermal impacts for varying tumor sizes 10 mm, 15 mm, and 20 mm through the application of the generalized dual-phase lag (GDPL) bioheat equation, a comprehensive approach that accounts for both temperature and heat flux phase lags.

## 2. Mathematical model

### 2.1 Problem definition

The biological structure analyzed in this study consists of five distinct layers: the rectal wall, a spacer composed of either HA or PEG, an intervening fat layer, the prostate, and the tumor. Laser thermal therapy is employed to ablate the tumor located within the prostate gland by delivering targeted heat. The introduction of HA or PEG spacers between the prostate and rectum is critical to minimizing the risk of thermal injury to sensitive surrounding tissues during the procedure. This study emphasizes the role of tissue porosity and the effects of vascular cooling within the tumor environment. A key innovation in this study is the application of the GDPL bioheat equation, which captures both the thermal phase lag between temperature gradient and heat flux, as well as the influence of vascular networks on tissue cooling. The model integrates the porous nature of biological tissues to provide a precise representation of heat transfer during laser therapy. The resulting temperature distributions are further used to assess the extent of the tumor ablation in the prostate.

Based on the experimental study of HA injection presented in Prada *et al.*[16] (2007), HA was injected in quantities ranging from 3 to 7 mL. Injecting HA into the perirectal fat increases the separation between the rectal wall and the prostate, creating an additional thermal protective layer, as illustrated in Fig. 1. This includes magnetic resonance image (MRI) images taken before and after HA injection, clearly showing an increased space around the rectum after the injection. Fig. 1 shows the injection of spacers to create a space between the prostate gland and the rectal wall in medical applications.

Laser treatment for prostate cancer, utilizing the GDPL bioheat equation, involves applying high temperatures to vaporize the tumor within the prostate, thereby destroying cancerous cells. Despite its efficacy, the high temperatures inherent in this treatment pose a significant risk of thermal damage to adjacent healthy tissues. To mitigate the risk, this study investigates the use of spacers, either HA or PEG, injected between the prostate and rectum. The primary objective is to mitigate thermal effects on the rectal wall, minimize rectal toxicity, and enhance patients' quality of life by minimizing bowel-related complications. According to the experimental results of Namakshenas *et al.* (2021),[15] a PEG spacer layer with a thickness of 2.59 mm was found to effectively protect the rectal wall from minor thermal damage. In this study, five distinct tissue domains are analyzed: 1. rectal wall (RW) 2. Gel (HA or PEG) 3. fat 4. prostate and 5. tumor, as shown in Fig. 2a. A 2D symmetric model of the five tissue domains was constructed based on MRI images. The model

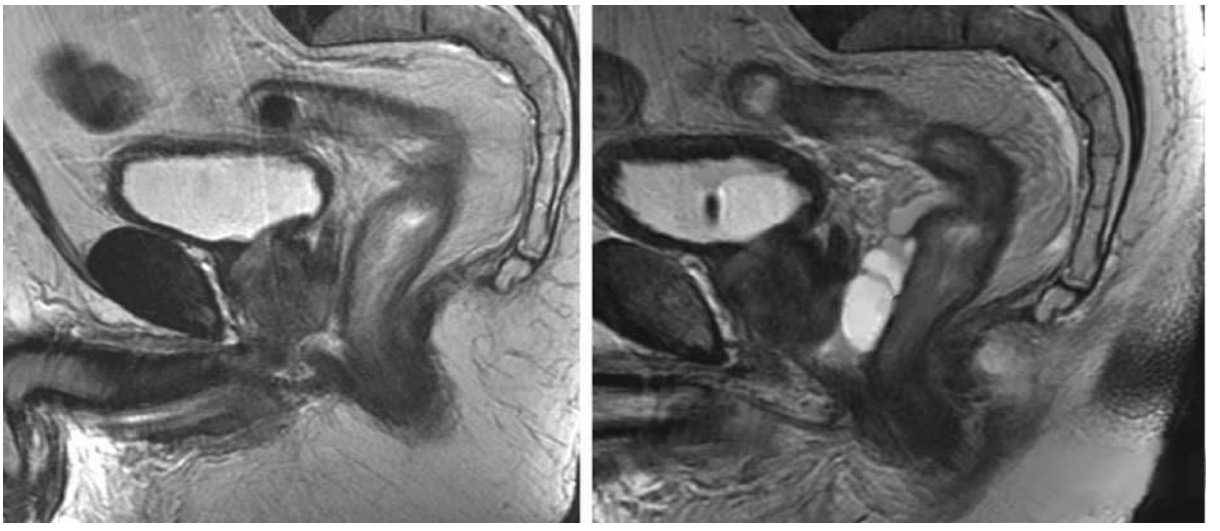

(a) before the injection HA (b) after the injection HA

**Fig. 1:** MRI image before and after the injection of Hyaluronic Acid (HA) during prostate cancer treatment.[16]

specifies the thickness of these layers as 2.6 mm, 2.59 mm, 5.7 mm, and 40 mm, respectively, as illustrated in Fig. 2b.[15,16] The computational domains #1 to #5 are displayed in Fig. 2b. Additionally, the porosity level of the tumor is set at 0.28, a critical parameter for accurate thermal modeling.[15] The simulation model incorporates detailed material properties for each layer, as outlined in Table 1.

### 2.2 Governing equations

The aim of this article is to examine the thermal damage in the prostate gland induced by laser radiation using the GDPL bioheat model presented in Eq. (1). This study considers heat conduction in both tissue and blood, along with the phase lag times related to heat flux and temperature gradients.[21]

$$(\rho C)'_{eff}\frac{\partial T}{\partial t} - k_{eff}\nabla^2 T = -(\rho C)_{eff}\tau_q\frac{\partial^2 T}{\partial t^2} + k_{eff}\tau_T\frac{\partial}{\partial t}(\nabla^2 T) + G(T_b - T) + \left(1 + \frac{\varepsilon\rho_b C_b}{G}\frac{\partial}{\partial t}\right)[(1-\varepsilon)Q_m + Q_{laser}] \quad (1)$$

where $\rho$ is the density, C is the specific heat, $\varepsilon$ represents tissue porosity, T is the temperature of the tissue, $Q_m$ and $Q_{laser}$ represent the metabolic heat source and the thermal energy generated by laser exposure, respectively. The subscript b indicates the blood parameters. $\tau_q$represents the phase lag time associated with heat flux. This indicates a delay during which the heat flux (the rate at which heat is transferred) responds to changes in temperature within the tissue, and $\tau_T$ represents the phase lag time related to the temperature gradient. This phase lag time refers to the delay in the response of the temperature gradient (the rate at which temperature changes over distance) to the heat or heat flux within the tissue.

Effective heat capacity and thermal conductivity, as shown in Eqs. (2) and (3), respectively, represent the thermal characteristics specific to cancerous tissue, taking into account the influence of the vascular network.[22]

**Table 1:** Material and thermal characteristics of each layer.[15,17-20]

| | Prostate | Tumor | Blood | Gel (HA) | Gel (PEG) | Rectal wall | Fat |
|---|---|---|---|---|---|---|---|
| $\rho\left(\frac{kg}{m^3}\right)$ | 1079 | 1079 | 1000 | 1800 | 1080 | 1027 | 930 |
| $C\left(\frac{J}{kg.K}\right)$ | 4000 | 4000 | 4180 | 2233 | 2440 | 2372 | 2770 |
| $k\left(\frac{W}{m.k}\right)$ | 0.52 | 0.52 | 0.51 | 0.272 | 0.23 | 0.39 | 0.21 |
| $w_b\left(\frac{1}{s}\right)$ | $5.6\times10^{-3}$ | $5.6\times10^{-3}$ | - | 0 | 0 | $5\times10^{-4}$ | $2\times10^{-4}$ |
| $\alpha\left(\frac{1}{m}\right)$ | 30 | | | | | | |
| $\alpha_s\left(\frac{1}{m}\right)$ | 8000 | | | | | | |
| g | 0.95 | | | | | | |

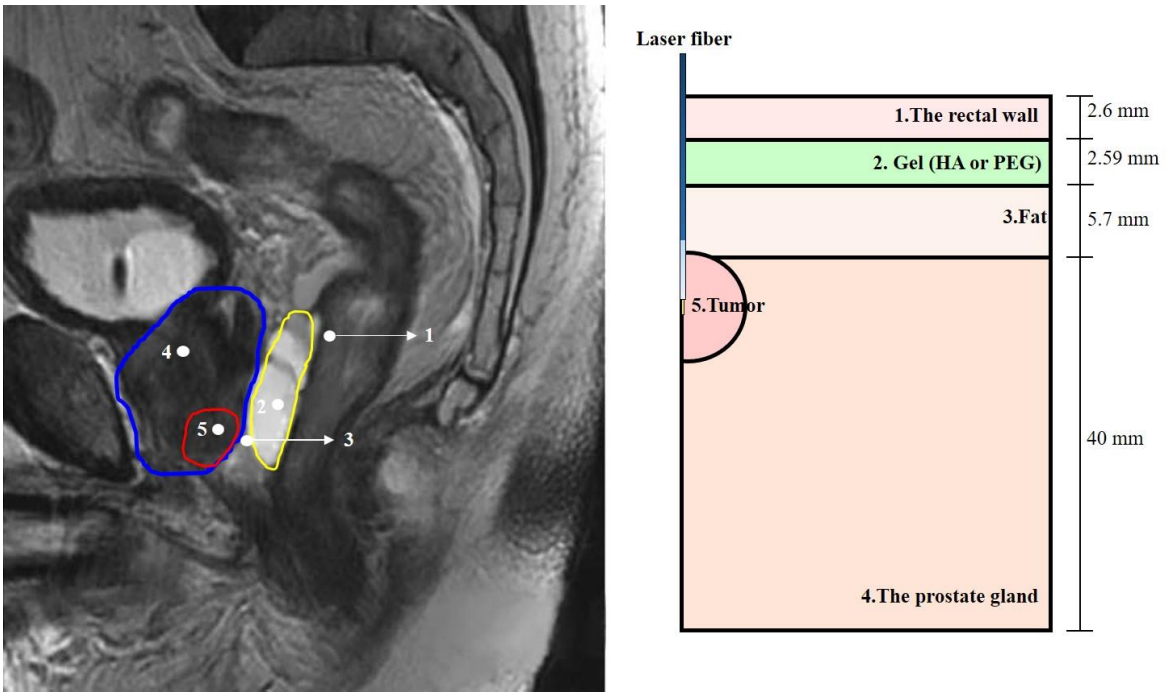


(a) MRI images (b) 2D symmetric model

**Fig. 2:** Physical model of the system. (a) represent the rectal wall, Gel (HA or PEG), Fat, the prostate gland, and the tumor, respectively. (b) The 2D symmetric model of the tissue layers was constructed based on MRI images, with computational domains #1 to #5 corresponding to the regions in the MRI image shown in (a).[16]

$$(\rho C)_{eff} = \varepsilon \rho_b C_b + (1-\varepsilon)\rho_t C_t \quad (2)$$

$$k_{eff} = \varepsilon k_b + (1-\varepsilon)k_t \quad (3)$$

From Eq. (1), it can be observed that there is a phase lag time for the spatial heat source. The phase lag times $\tau_T$ and $\tau_q$ can be calculated with Eqs. (4) and (5), which are determined using the equation. The delay is a function of tissue porosity ($\varepsilon$), the heat capacities ratio of tissue to blood ($C_{tb} = C_t/C_b$), the thermal conductivity ratio of tissue and blood ($k_{tb} = k_t/k_b$), The coupling factor between blood and tissue, (G), and the energy stored in the blood ($\rho_b C_b$).

$$\tau_q = \frac{\varepsilon\,(1-\varepsilon)}{\left[\frac{\varepsilon}{C_{tb}}+(1-\varepsilon)\right]}\frac{\rho_b C_b}{G} \quad (4)$$

$$\tau_T = \frac{\varepsilon\,(1-\varepsilon)}{\left[\frac{\varepsilon}{k_{tb}}+(1-\varepsilon)\right]}\frac{\rho_b C_b}{G} \quad (5)$$

Many studies have assumed a constant blood temperature during laser irradiation, overlooking the fact that both tissue and blood actually experience a temperature increase. In this research, we account for the temperature variations in both tissue and blood during laser exposure, as outlined in Eq. (6). The blood temperature is subject to a transient process during the heat exchange between blood and tissue.[23-24]

$$\varepsilon \rho_b C_b \frac{\partial T_b}{\partial t} = G(T_t - T_b) \quad (6)$$

Heat convection among the vascular region, extravascular region, and blood flow plays a key role in heat distribution. The coupling factor (G) in Eq. (7) represents the combined convection between tissue and blood. In this equation, the first term accounts for convection, where $d_b$ is the average diameter of blood vessels in the prostate, which is approximately 0.9 mm. where $w_b$ is the blood flow rate. Therefore, the coupling factor can be calculated, provided that the porosity, vessel diameter, and blood flow rate are known. In this context, the Nusselt number is typically approximated as Nu = 4.93.

$$G = \frac{4\varepsilon k_b}{d_b^2} Nu + w_b C_b \quad (7)$$

Moreover, the increase in temperature from laser irradiation is sufficient to cause water evaporation within the tissue. Consequently, the energy stored effectively is adjusted, as shown in Eq. (8), taking into account the water evaporation at temperatures above 100 °C. In this equation, $h_{fg}$ represents the latent heat associated with water evaporation, and $\rho_w$ denotes the volume fraction of water retained in the tissue during treatment, which is temperature-dependent.

$$(\rho C)'_{eff} = (\rho C)_{eff} - \frac{h_{fg}}{\rho}\frac{\partial \rho_w}{\partial T} \quad (8)$$

The change in water volume follows Eq. (9). [17]

$$\rho_w = \begin{cases} 0.778\left(1 - exp\left(\frac{T-106}{3.42}\right)\right) \because T \le 103 \\ (0.0289T^3 - 8.924T^2 + 919.6T - 31573) \times 10^{-2} \because 103 < T \le 103 \\ 77.8\, exp\left(-\frac{T+80}{34.37}\right) \because T > 104 \end{cases} \quad (9)$$

The GDPL model is employed to evaluate thermal effects in both cancerous and healthy biological tissues, whereas the Pennes model governs the thermal dynamics in the spacer, fat layers, and rectal wall. The laser's heat output is modeled with a Gaussian distribution, as detailed in Eq. (10). $Q_{laser}$ (W/m$^3$) represents the energy absorbed by the tissue, following the principles of the Beer-Lambert law. This model considers P as the laser power in continuous output mode, $r_f$ is the radius of the optical fiber, and $\alpha_{eff}$ as the tissue's effective attenuation coefficient. In the laser-tissue interaction, the laser energy is distributed throughout the targeted area. Eq. (11) defines the effective attenuation coefficient, incorporating both the scattering coefficient ($\alpha_s$) and the anisotropy factor (g) of the tissue. Clinical data on tissue-ablative laser treatments suggest laser powers typically range between 4 W and 15 W.[17,25]

$$Q_{laser} = \alpha_{eff} \frac{P}{2\pi(r_f/3)^2} exp\left(-\left(0.5\left(\frac{r^2}{(r_f/3)^2}\right) + \alpha_{eff} Z\right)\right) \quad (10)$$

$$\alpha_{eff} = \sqrt{3\alpha\left(\alpha + \alpha_s(1-g)\right)} \quad (11)$$

### 2.3 Boundary conditions

The simulation model was developed from MRI images, illustrating a multi-layered structure as depicted in Fig. 2. This structure includes five distinct layers: rectal wall (RW), Gel (HA or PEG), the fat layer, the prostate, and the tumor, along with the positioning of the laser fiber. Tumor diameters were modeled at 10 mm, 15 mm, and 20 mm. A gel spacer, introduced into the anterior rectal fat cavity, serves as a thermal barrier with a thickness of 2.59 mm to protect the rectal wall tissue from heat-induced damage.[15] The system's initial conditions set the temperatures of both blood and tissue at 37 °C, with these and other boundary conditions displayed in Fig. 3. During laser irradiation, tissue, and blood are subjected to a gradual increase in temperature over time. In this study, the temperature changes in the tissue and blood around the tumor and prostate are taken into consideration. The laser fiber, which has a radius of 150 µm, is strategically placed within the tumor to deliver the energy necessary for its ablation. Thermal insulation is applied along the sidewalls of the laser fiber and across the tissue surface, with the exception of the rectal wall's outer surface, which is regulated at a constant 37 °C.

## 3. Method

In this research, a mathematical model was developed to investigate the thermal effects on the rectal wall during laser therapy for prostate cancer, utilizing HA and PEG spacers positioned between the rectal wall and the tumor. The finite element method (FEM) was utilized, with the tissue model created using COMSOL™ Multiphysics (version COMSOL 6.1.0.282). Grid intensity analysis was conducted to determine the optimal number of elements, with approximately 35,000 elements found to be the most suitable (as shown in Fig. 4). Increasing the number of elements beyond this did not enhance the model's accuracy. This research explores strategies to minimize the thermal impact on the tumor area affected by laser irradiation by using HA and PEG spacers between the rectum and the tumor, aiming to minimize unwanted damage from laser treatment. The model was validated against previous research. The fundamental parameters of the tissue layers were incorporated into the model, as detailed in Table 1.

The study compared the use of HA, PEG spacers, and no gel spacers, with the thickness of HA and PEG set at 2.59 mm. The tumor sizes considered had diameters of 10 mm, 15 mm, and 20 mm. The laser was operated in pulse mode with an exposure time of 10 s, a laser power of 4 W, a wavelength of 1,064 nm, and a laser beam radius of 150 µm. The simulation was conducted over 240 s to record the temperature changes in the rectal wall. The study compared and illustrated the

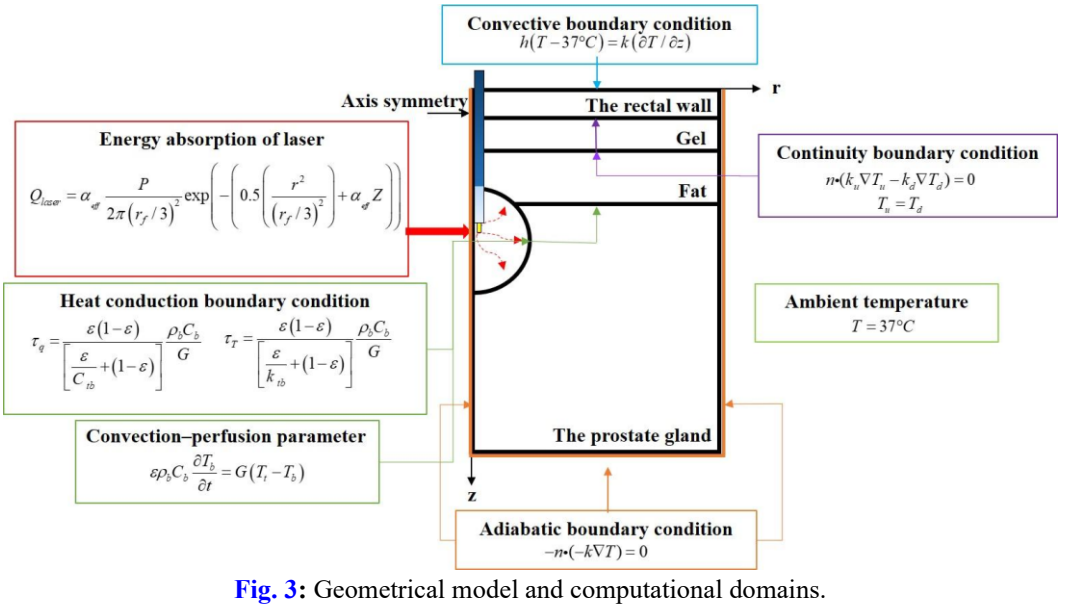


**Fig. 3:** Geometrical model and computational domains.

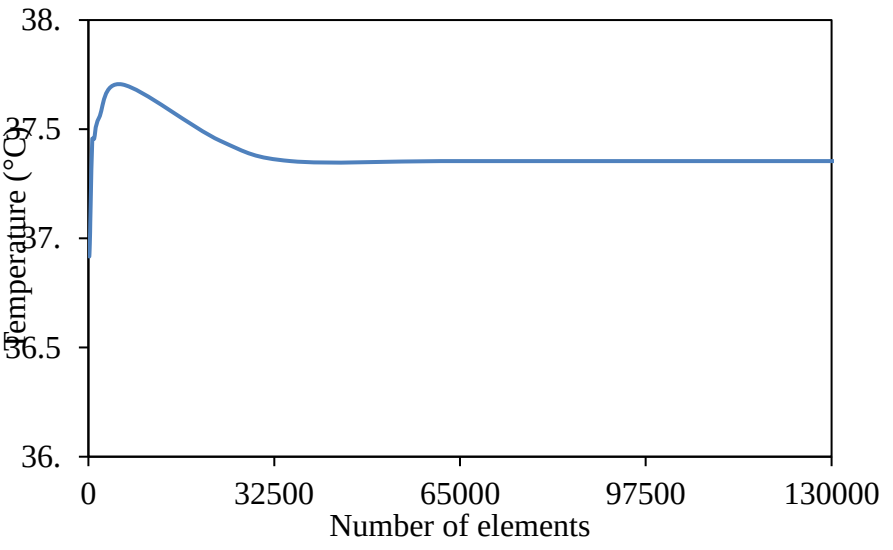


**Fig. 4:** Mesh independence study showing convergence with the increasing number of elements.

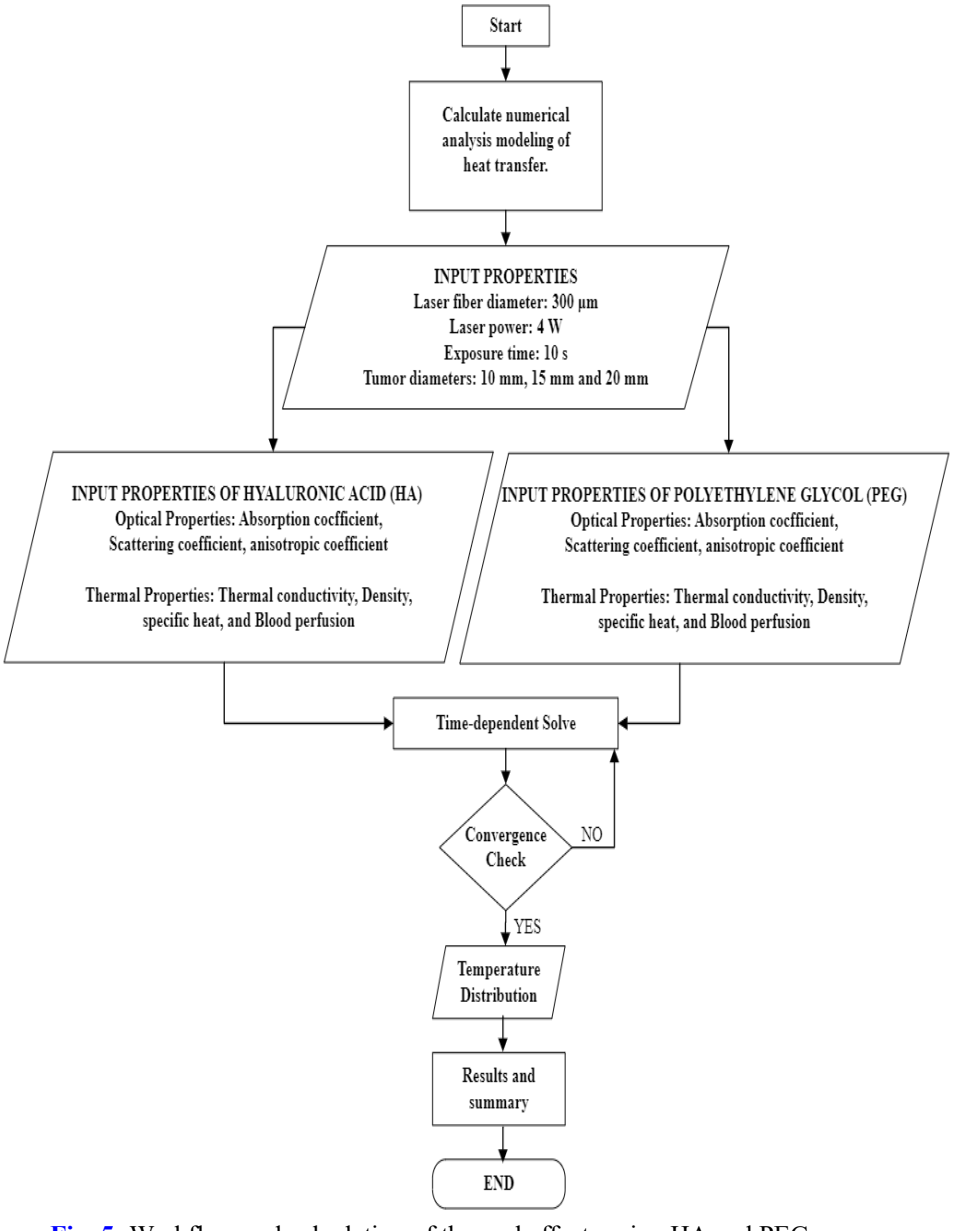


**Fig. 5:** Workflow and calculation of thermal effects using HA and PEG spacers.

thermal differences in the rectal wall, aiming to identify a maximum temperature that should not exceed 60 °C to prevent rectal wall damage and ideally should remain below 42 °C to avoid injury to the biological tissue, The procedure and thermal impact calculations using HA and PEG spacers are illustrated in Fig. 5.

## 4. Model verification

To validate the current numerical model, the results were compared with those of Namakshenas *et al.* (2021).[15] An analytical solution for the GDPL model was developed. The validation case utilized axial symmetry of the tissues, including rectal wall tissue, fat layer, and prostate gland, which were irradiated with a laser. The computer model was simulated with a wavelength of 1064 nm, a laser power of 4 W, with a duration of 10 seconds. Without the use of a PEG spacer, the current results in Fig. 6 show a clear consistency in the temperature distribution over time with the present solution.[15] This close agreement supports the accuracy of the current numerical model.

## 5. Result and discussion

This article presents an approach to mitigating the thermal effects caused by prostate cancer treatment using laser radiation by comparing the use of HA and PEG spacers injected between the rectum and the prostate gland to reduce unwanted damage. The study also includes a thermal analysis that explains the porous structure of the prostate tumor. In this research, the generalized dual-phase-lag mathematical model was employed to investigate the temperature distribution and assess the impact of tumor size when using HA and PEG spacers, as well as in the absence of any spacer.

### 5.1 Observing the thermal response in rectal wall tissues exposed to laser irradiation

Fig. 7 illustrates the relationship between temperature and time, depicting the thermal response of the tissue in the rectal wall area with a tumor diameter of 10 mm. The laser operates at 4 W, with an exposure duration of 10 seconds. The simulation, depicted in Fig. 7, spanned 240 seconds to capture the temperature fluctuations throughout this period for both PEG and HA spacers, as well as without a spacer. The results indicate that, without a Gel spacer, the rectal wall reached a maximum temperature of 38.84 °C at t = 119 s. When HA and PEG spacers were used, the graph displayed a longer delay with lower temperatures than the No Spacer condition. For PEG and HA, the maximum temperatures reached 37.67 °C at t = 190 s and 37.74 °C at t = 190 s, respectively. After the laser radiation was deactivated at t = 10 s, the tissue temperature immediately decreased. However, the temperature within the rectal wall continued to increase for several seconds subsequent to the termination of laser radiation.

A temperature threshold of 42 °C is known to signify the onset of the injury in biological tissue. Fig. 8 compares the maximum rectal wall temperature with a 10 mm tumor under three conditions: No Spacer, PEG, and HA. The results demonstrate that the use of HA and PEG spacers reduced the rectal wall temperature by 3.0% and 2.83%, respectively, compared to the No Spacer condition. This reduction is attributed to the relatively low thermal conductivity of HA and PEG, which are frequently employed in biological and medical applications due to their non-toxic properties and compatibility with human tissues, along with their capacity to absorb and retain water within their structures.

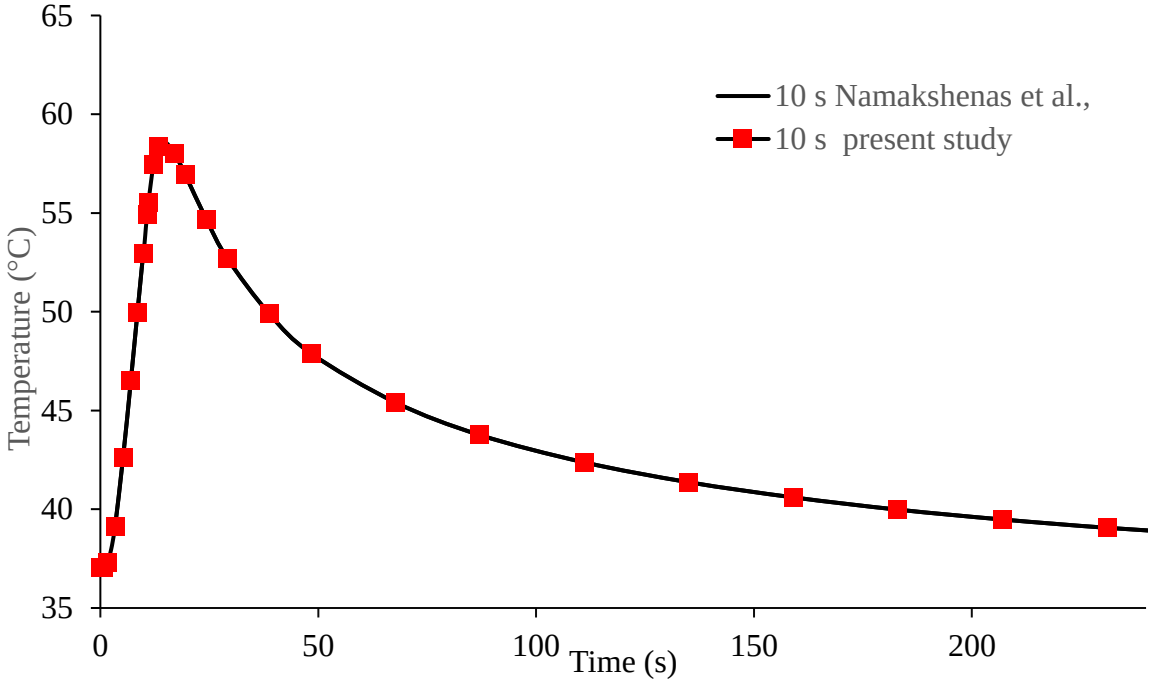


**Fig. 6:** Comparison of rectal wall temperature distribution without PEG between the study by Namakshenas *et al.* (2021) and the present study.

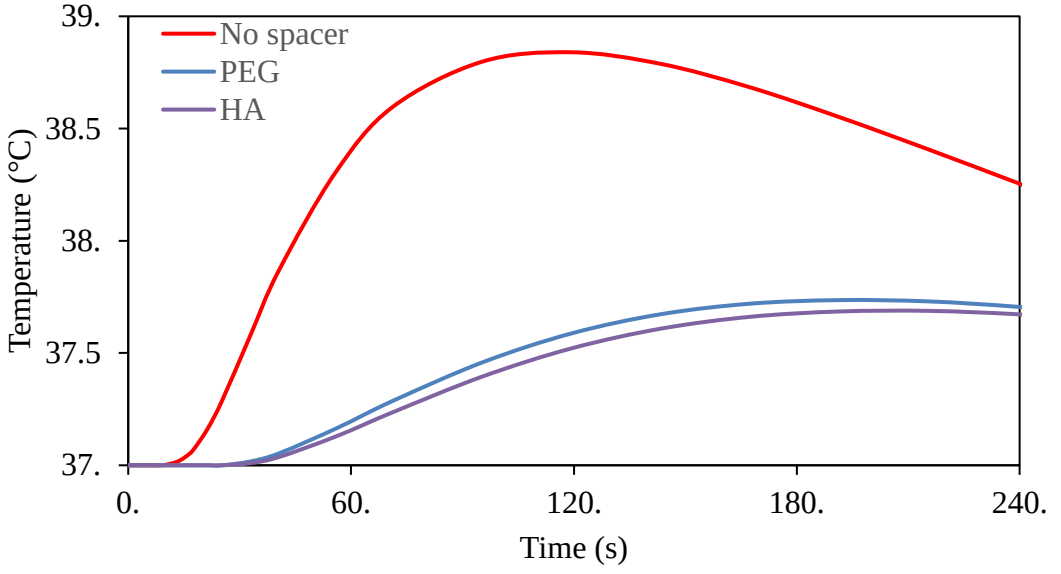


**Fig. 7:** Temperature profiles over time for the rectal wall with a tumor diameter of 10 mm, comparing No Spacer, PEG, and HA.

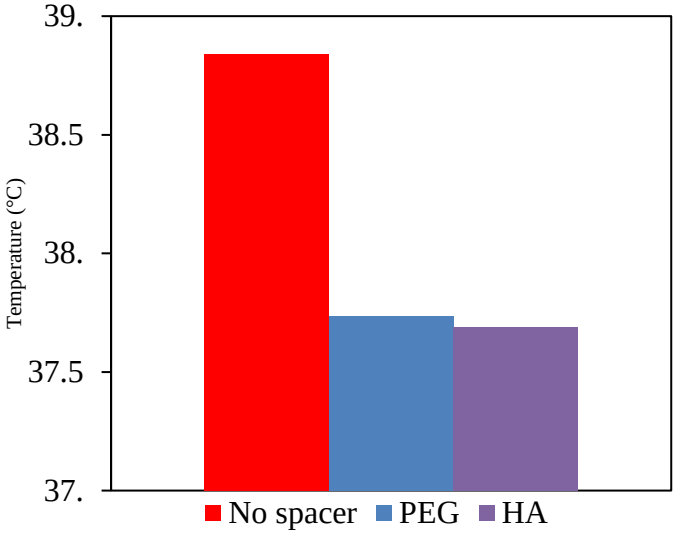


**Fig. 8:** Peak temperature in the rectal wall with a tumor diameter of 10 mm, comparing No Spacer, PEG, and HA.

Fig. 9 presents a graph illustrating the relationship between temperature and time, showing the thermal response of the rectal wall tissue when the tumor diameter is 15 mm. The graph records temperature changes over a 240 s period for both PEG and HA spacers and in the absence of a spacer. With the tumor size increased by 5 mm while maintaining the same tumor center position, the simulation results indicate that without a spacer, the maximum temperature reached 45.0 °C at t = 44 s. When HA and PEG spacers were used, the maximum temperatures were 39.06 °C at t = 130 s and 39.22 °C at t = 130 s, respectively.

As shown in Fig. 10, the maximum rectal wall temperature with a 15 mm tumor is under three conditions: No Spacer, PEG, and HA. The results demonstrate that the use of HA and PEG spacers reduced the rectal wall temperature by 13.2% and 12.8%, respectively, compared to the No Spacer condition. As the tumor size increases, the temperature of the rectal wall tissue also rises due to the closer proximity of the rectal wall to the heat transfer from the laser radiation. However, the presence of HA and PEG spacers effectively reduces the rectal wall temperature.

In Fig. 11, the relationship between temperature and time shows the thermal response of the rectal wall tissue over 240 s when the tumor diameter is 20 mm, with the tumor center position remaining the same. The simulation results indicate that without a spacer, the temperature at the rectal wall for a 20 mm tumor is higher than for 15 mm and 10 mm tumors, respectively. The larger tumor size results in closer proximity to the rectal wall, leading to faster and greater heat distribution. The maximum temperature at the wall of the rectum for the 20 mm tumor reached 164.22 °C at t = 10 s. When HA and PEG spacers were used, the maximum temperatures reached 42.46 °C at t = 52 s and 42.89 °C at t = 52 s, respectively. It is noteworthy that with spacers, the temperature delay was extended after the laser radiation was deactivated at t = 10 s, with a 42 s difference in the peak temperature between the No Spacer and the HA and PEG spacers.

Fig. 12 compares the Peak temperature in the rectal wall temperature with a 20 mm tumor under three conditions: No Spacer, PEG, and HA. The results demonstrate that the use of HA and PEG spacers reduced the rectal wall temperature by 74.1% and 73.9%, respectively, compared to the No Spacer condition. It is evident that the use of HA and PEG spacers effectively reduces the rectal wall temperature, with HA being slightly more effective than PEG. The experimental results show that HA consistently reduces rectal wall temperature more effectively than PEG throughout the simulation. The thermal conductivity of HA and PEG are similar, but a significant difference lies in their densities, with HA having a higher density than PEG. This higher density allows HA to absorb and retain more thermal energy, making it more efficient in reducing heat transfer to the surrounding tissues.

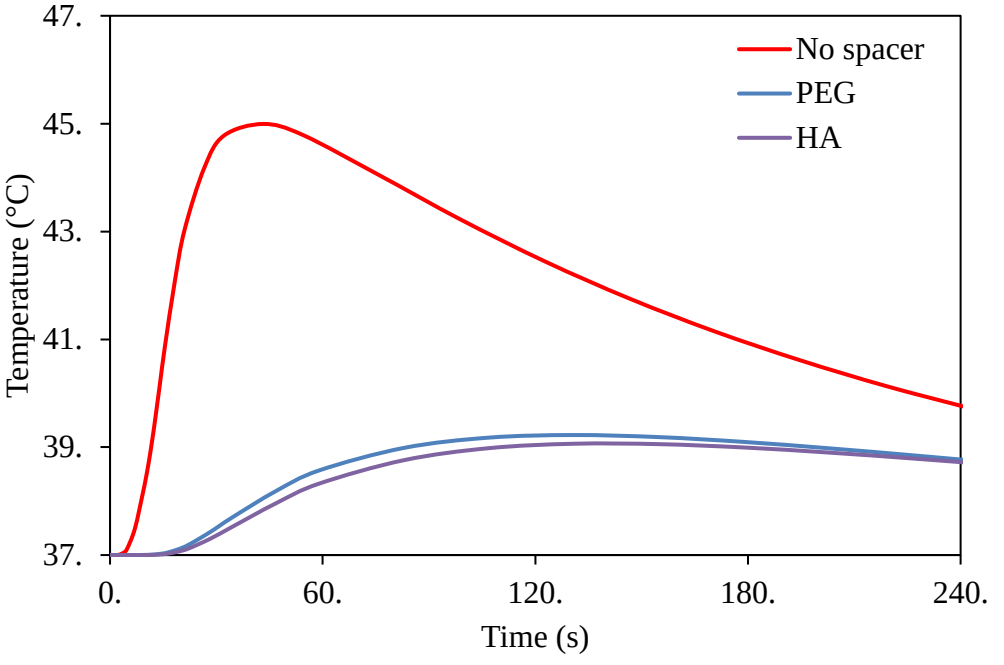


**Fig. 9:** Temperature profiles over time for the rectal wall with a tumor diameter of 15 mm, comparing No Spacer, PEG, and HA.

### 5.2 Analysis of thermal damage distribution across tumors of varying sizes

As shown in Fig. 13 compares thermal damage distribution in tumors at 70 s as their size increases to 10 mm, 15 mm, and 20 mm with HA used as a spacer. The comparison is made at t = 70 s, the point at which tumor destruction is complete, while maintaining the same central position within the prostate gland. As the tumor size increases and becomes closer to the rectal wall, the laser light intensity and exposure time remain constant at 4 W and 10 s, respectively. Thermal therapy typically aims for temperatures between 55 and 60 °C or higher to rapidly destroy cancer cells, while minimizing irreversible damage to normal cells (or healthy tissue). This temperature range induces protein denaturation, irreversible DNA damage, blood coagulation, and immediate cell death.[26]

In Fig. 13, at the end of the tumor ablation process at t = 70 s, the simulation shows that the 10 mm tumor was completely destroyed by the heat from the laser by t = 60 s. In contrast,

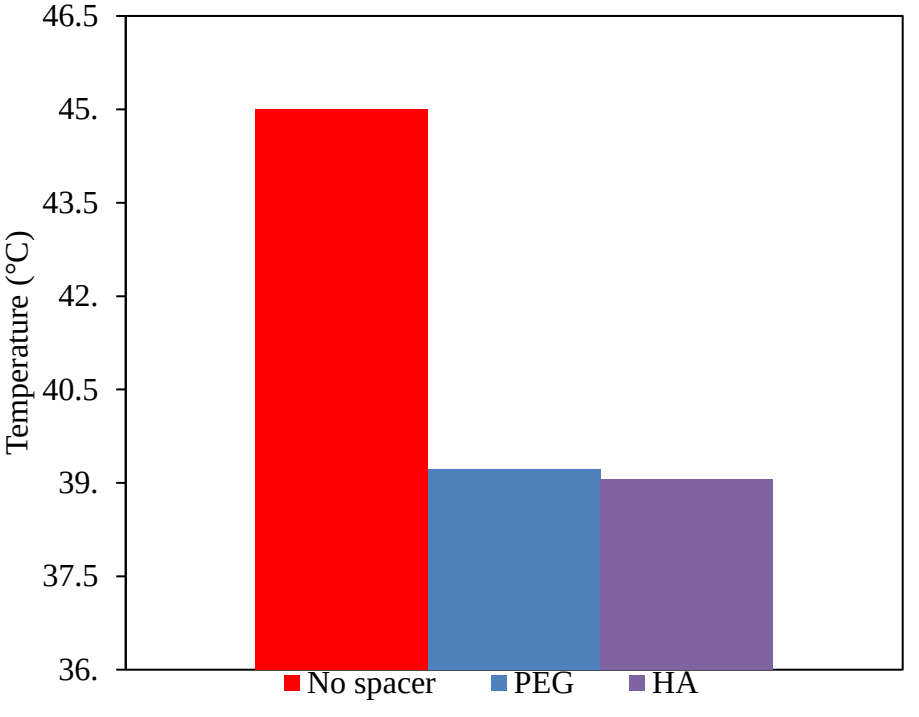


**Fig. 10:** Peak temperature in the rectal wall with a tumor diameter of 15 mm, comparing No Spacer, PEG, and HA.

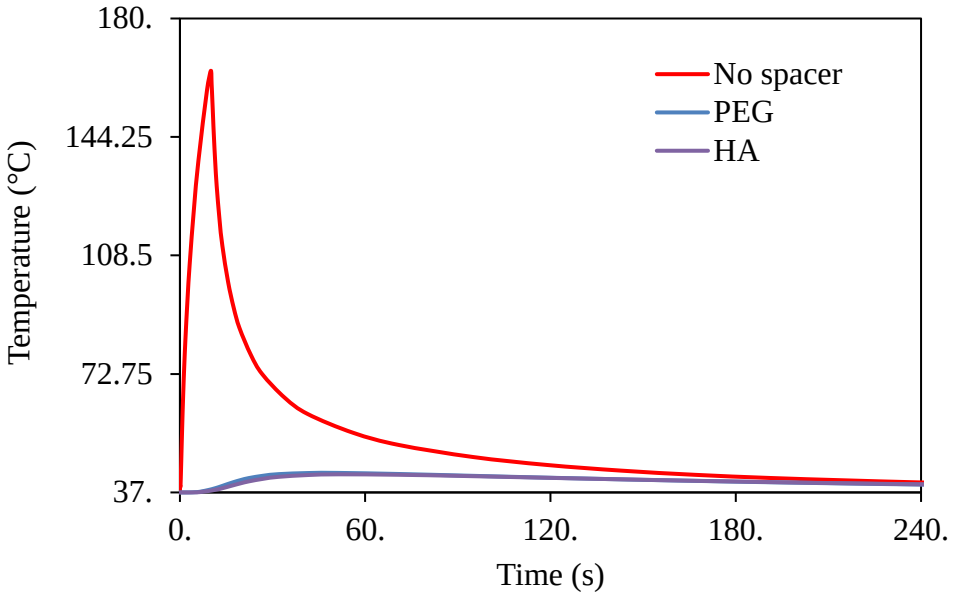


**Fig. 11:** Temperature profiles over time for the rectal wall with a tumor diameter of 20 mm, comparing No Spacer, PEG, and HA.

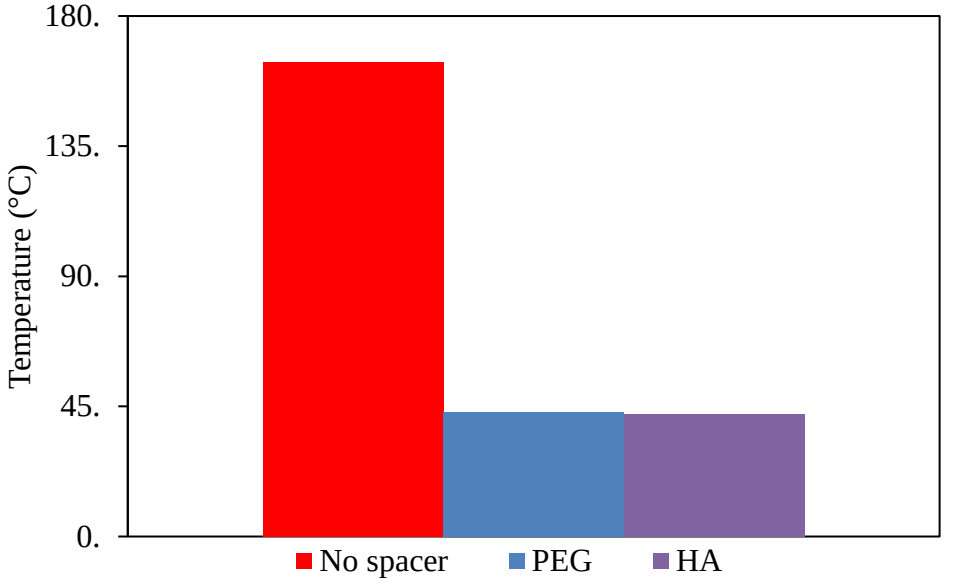


**Fig. 12:** Peak temperature in the rectal wall with a tumor diameter of 20 mm, comparing No Spacer, PEG, and HA.

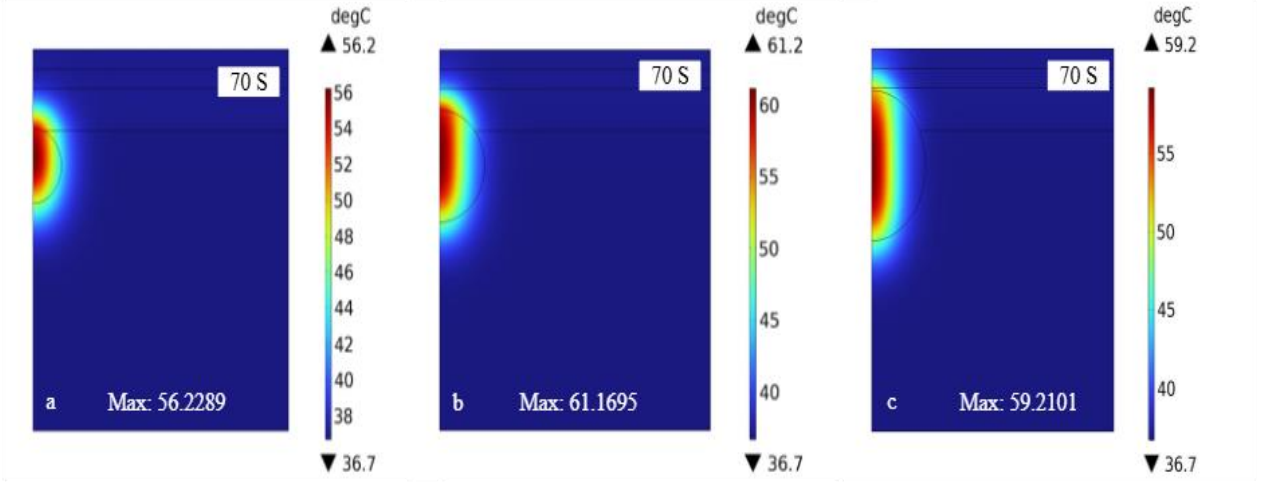


**Fig. 13:** The thermal damage distribution across tumors of different sizes: (a) 10 mm, (b) 15 mm, and (c) 20 mm, with complete tumor elimination occurring at t = 70 seconds.

for tumors measuring 15 mm and 20 mm, complete destruction occurred at t = 70 s, indicating that the heat could not entirely eliminate the tumor within the treatment time. Therefore, when dealing with larger tumors, the heating duration should be extended or the laser power increased to ensure complete tumor elimination. However, doing so also increases the thermal impact on the rectal wall, as prolonged heating can affect the surrounding healthy tissues. Consequently, the removal of large tumors may not be achievable in a single session.

### 5.3 Effect of HA spacer injection

This section presents the temperature distribution of the entire tissue in the prostate cancer treatment model using lasers with and without HA and PEG spacers. The laser power is set 4 W, and the laser application time is 10 s. The tumor size is 15 mm, and the simulation will run for 240 s. Tumor destruction begins at t = 10 s and ends at t = 70 s. The tumor undergoes thermal damage over a period of 70 s, a duration that delineates the boundary of the rectal wall at increased risk of thermal injury. After 70 s, the tissue temperature begins to decrease, marking the end of cancer cell destruction. Fig. 14 illustrates the temperature distribution in the model without a spacer. At t = 10 s, the maximum tissue temperature reaches 1087 °C and tends to decrease until t = 70 s, where the maximum tissue temperature is 61 °C by the end of the treatment.

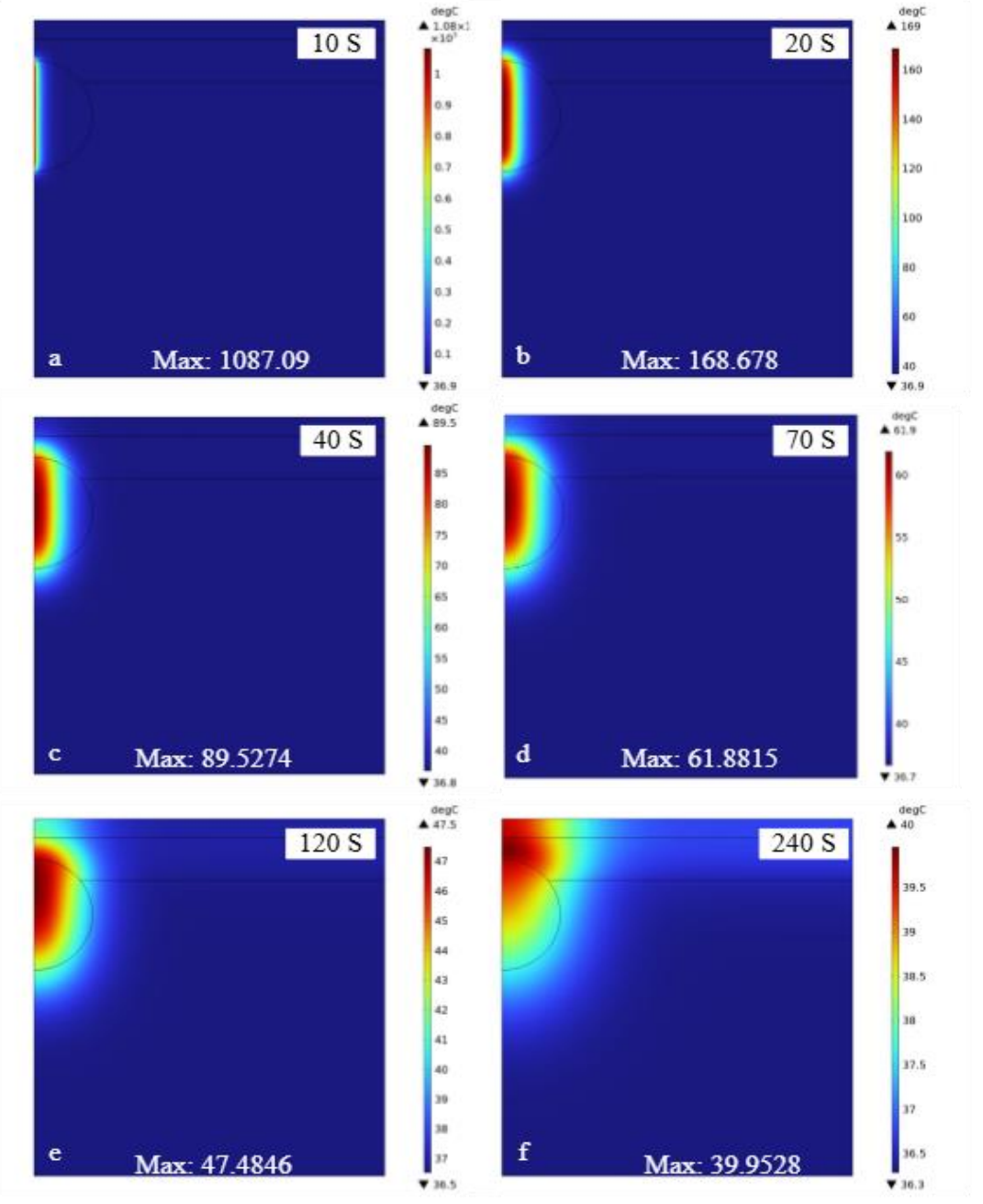


**Fig. 14:** Temperature distribution within a 15 mm diameter tumor without a spacer, recorded at intervals of 10 s, 20 s, 40 s, 80 s, 120 s, and 240 s of a-f.

Fig. 15 shows the temperature distribution in the prostate cancer treatment model using lasers with HA injected to create a spacer between the rectal wall and the prostate. The laser power is set at 4 W, and the laser application time is 10 s. Tumor destruction starts at t = 10 s and ends at t = 70 s. The tumor is exposed to heat damage for 70 s. At 10 seconds, the maximum tissue temperature recorded is 992 °C. This time frame represents the boundary of the rectum wall that is likely to experience increased thermally induced damage. However, with the HA spacer, the temperature decreases by 8.74% compared to the model without a spacer, which leads to a reduction in the heat affecting the rectal wall.

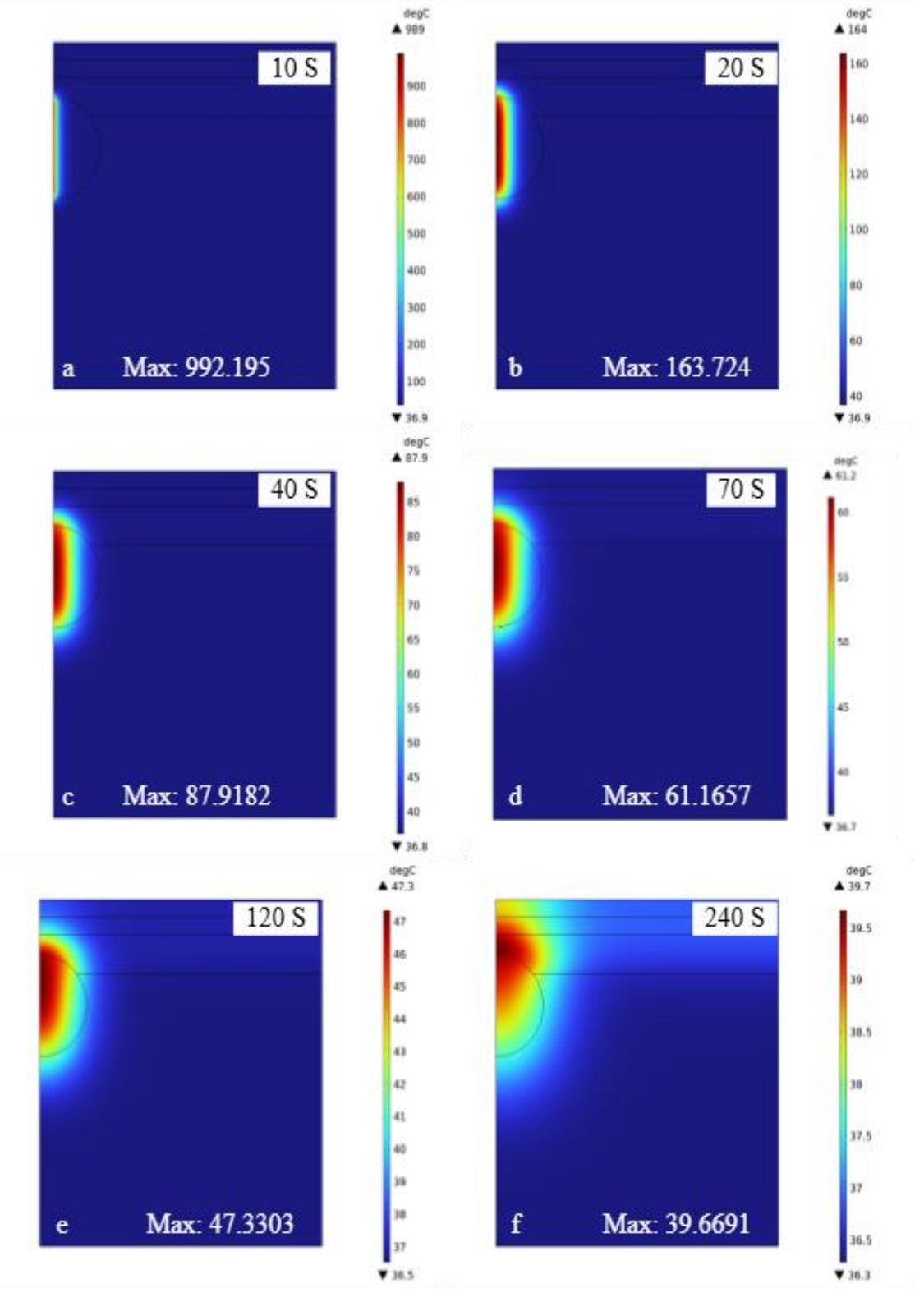


**Fig. 15:** Temperature distribution within a 15 mm diameter tumor with an HA spacer at time intervals of 10 s, 20 s, 40 s, 80 s, 120 s, and 240 s of a-f.

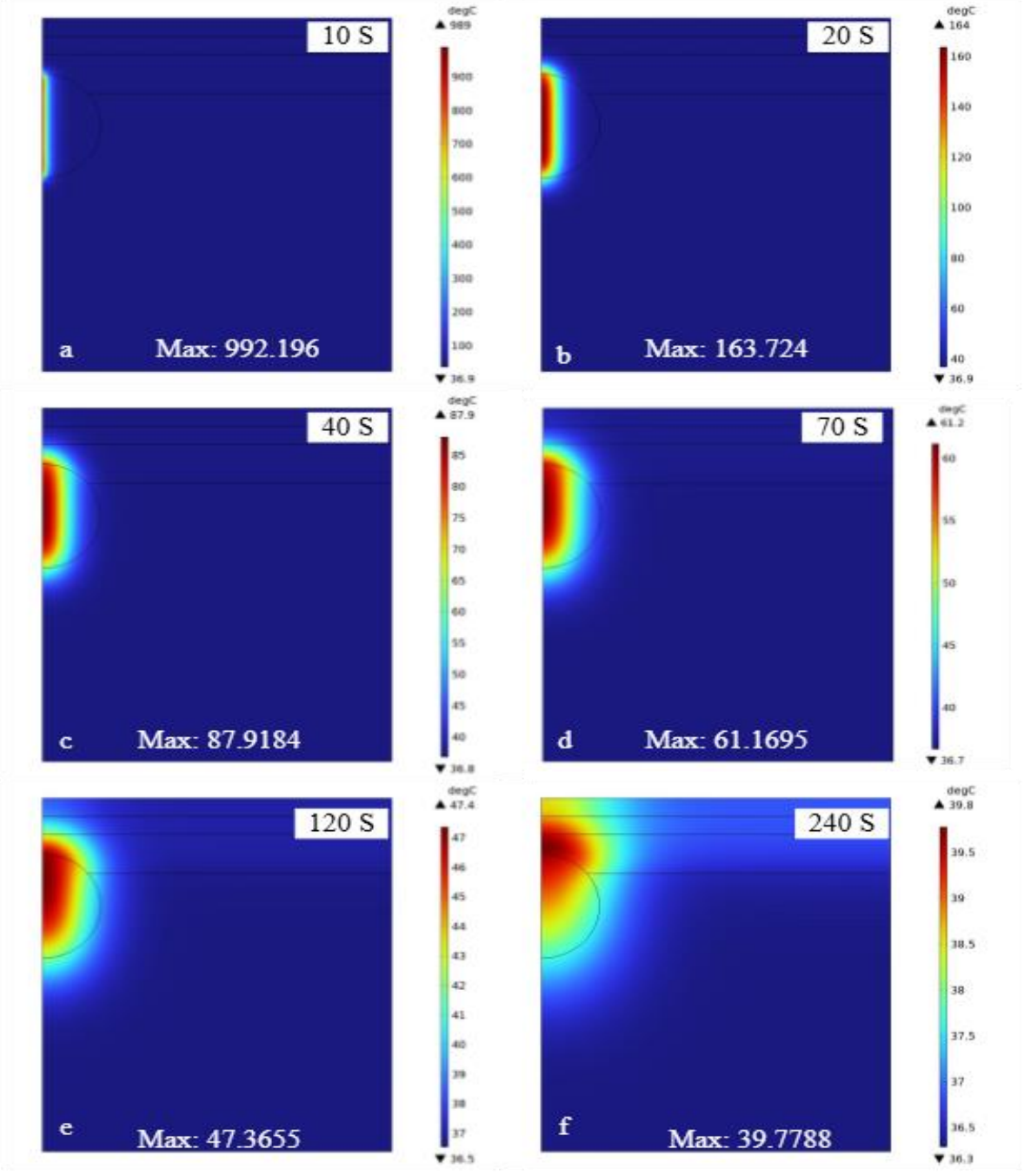


**Fig. 16:** Temperature distribution in a 15 mm diameter tumor with a PEG spacer at time intervals of 10 s, 20 s, 40 s, 80 s, 120 s, and 240 s of a-f.

Similarly, Fig. 16 shows the temperature distribution with PEG injected as a spacer. At t = 10 s, the maximum tissue temperature is 992 °C. This demonstrates that injecting PEG as a spacer also reduces the maximum tissue temperature by the same amount as HA, which is 8.74%.

### 5.4 Discussion

Laser vaporization therapy is an innovative approach for treating prostate cancer, utilizing short-term heating to destroy cancer cells while aiming to minimize damage and side effects to the rectal wall. However, when tumors are located close to the rectal wall and are larger in size, the risk of injuring adjacent healthy tissues, such as the rectum, increases .Various materials have been evaluated as spacers to separate the rectal wall from the prostate, such as HA, PEG, hydrogels, collagen, and saline-filled rectal balloon implants. Among these, stable HA gel has recently attracted attention due to its ability to be molded into specific shapes and maintain these forms while retaining flexibility, a characteristic not observed in PEG hydrogels.[27] Therefore, HA was chosen for comparison in this study regarding its thermal effects. Simulation results indicate that HA injection significantly reduces the maximum

temperature in the rectal wall compared to no spacer. For tumor sizes of 10 mm, 15 mm, and 20 mm, temperature reductions of 3.0%, 13.2%, and 74.1% were observed, respectively. This reduction in temperature is more effective than PEG, which reduced the temperature by 2.83%, 12.8%, and 73.9%, respectively, compared to no spacer. Although the thermal conductivity values of HA and PEG are low and similar, HA has a higher density than PEG, which allows HA to absorb and retain more thermal energy, making it more effective in reducing heat transfer to surrounding tissues.

In practice, HA as a rectal spacer is safe, easy to use, and effective in achieving the expected results. It is likely to improve patient outcomes after radiation without acute toxicity from injection. The user-friendly properties of HA enhance precise placement, ensuring optimal separation and symmetry. Unlike PEG hydrogels, HA can be shaped as required and maintains its form while remaining flexible. PEG spacers have less flexibility, which increases the risk of long-term gastrointestinal side effects compared to HA spacers.[27] HA remains in the rectal area without changing shape or being absorbed for up to 10–12 months before being reabsorbed by the body. PEG hydrogels maintain their integrity for 3 months before degrading. Across all user experience levels, HA has demonstrated a significant reduction in rectal toxicity and improved patient outcomes.[28-30]

## 6. Conclusion

In the simulation of prostate cancer treatment with lasers, this study utilizes the Generalized Dual-Phase-Lag model to analyze the thermal effects on the rectal wall. The focus is on comparing the efficacy of HA and PEG as spacers injected between the rectum and the tumor in mitigating these thermal effects. Notably, HA is being used for the first time in a numerical model as a rectal spacer in this context. The results demonstrate that HA injection significantly lowers the maximum temperature in the rectal wall compared to no spacer. For tumor sizes of 10 mm, 15 mm, and 20 mm, the temperature was reduced by 3.0%, 13.2%, and 74.1%, respectively. This temperature reduction is more effective than PEG because HA has a higher density than PEG, which enables it to absorb and retain more thermal energy. The simulation indicates that for a 10 mm tumor, the heat from the laser can completely destroy the tumor by t = 60 s. In contrast, for tumors of 15 mm and 20 mm, the heat is insufficient to destroy the tumor entirely by the end of the treatment. Therefore, for larger tumors, the heating duration should be extended compared to smaller tumors to ensure complete tumor destruction. However, the increased heating duration also leads to higher thermal effects on the rectal wall, as prolonged heating affects the surrounding healthy tissue. This study can serve as a guideline for reducing damage to the rectal wall during laser therapy for prostate tumors, particularly when the tumors are situated near the rectal wall. Additionally, the study also investigates the impact of varying the fat layer thickness on the rectal wall temperature when using HA as a spacer. If successful, this research will provide valuable insights for physicians, aiding in the planning and optimization of laser therapy treatments to minimize thermal damage and improve patient outcomes.

## Acknowledgments

This work was supported by the Thailand Science Research and Innovation Fundamental Fund fiscal year 2025 (Contract No. TUFF43/2568), Graduate Studies Faculty of Engineering, Thammasat School of Engineering (2023-2026), Thammasat University Thailand and this study was supported by Thammasat University Research Fund, Contract No TUFT 35/2567. The authors wish to express their gratitude to the Adult and Elderly Nursing Department, Faculty of Nursing, Thammasat University, Thailand, Department of Radiology, Faculty of Medicine, Prince of Songkla University, Thailand and Department of Mechanical and Industrial Engineering at Rajabhat Sakon Nakhon University. The researcher would like to express profound gratitude and utmost respect to those who have continuously provided guidance, support, advice, and corrections throughout the course of this work.

## Conflict of Interest

There is no conflict of interest.

## Supporting Information

Not applicable.

## References

[1] A. Hinchliffe, J. Alguacil, W. Bijoux, M. Kogevinas, F. Menegaux, M.-E. Parent, B. Pérez Gomez, S. Uuksulainen, M. C. Turner, Occupational heat exposure and prostate cancer risk: A pooled analysis of case-control studies, *Environmental Research*, 2023, **216**, 114592, doi: 10.1016/j.envres.2022.114592.

[2] K. D. Miller, L. Nogueira, T. Devasia, A. B. Mariotto, K. Robin Yabroff, A. Jemal, J. Kramer, R. L. Siegel, Cancer treatment and survivorship statistics, *CA*, 2022, **72**, 409-436, doi: 10.3322/caac.21731.

[3] T. J. Wilt, M. K. Brawer, K. M. Jones, M. J. Barry, W. J. Aronson, S. Fox, J. R. Gingrich, J. T. Wei, P. Gilhooly, B. Mayer Grob, I. Nsouli, P. Iyer, R. Cartagena, G. Snider, C. Roehrborn, R. Sharifi, W. Blank, P. Pandya, G. L. Andriole, D. Culkin, T. Wheeler, Prostate Cancer Intervention versus Observation Trial Study Group, Radical prostatectomy versus observation for localized prostate cancer, *New England Journal of Medicine*, 2012, **367**, 203-213, doi: 10.1056/NEJMoa1113162.

[4] E. Walser, A. Nance, L. Ynalvez, S. Yong, J. S. Aoughsten, E. J. Eyzaguirre, S. B. Williams, Focal laser ablation of prostate cancer: results in 120 patients with low- to intermediate-risk disease, *Journal of Vascular and Interventional Radiology*, 2019, **30**, 401-409.e2, doi: 10.1016/j.jvir.2018.09.016.

[5] N. Manuchehrabadi, L. Zhu, Gold nanoparticle-based laser photothermal therapy, *Handbook of Thermal Science and Engineering*, 2017, 1-33, doi: 10.1007/978-3-319-32003-8_69-1.

[6] A. Dinda, J. Acharya, D. Bhanja, S. Nath, Local thermal non-equilibrium bioheat transfer model for interstitial hyperthermia treatment of tumour cell: A numerical approach, *Journal of Thermal Biology*, 2022, **110**, 103368, doi: 10.1016/j.jtherbio.2022.103368.
[7] J. Saemathong, N. Pannucharoenwong, V. Mongkol, S. Vongpradubchai, P. Rattanadecho, Analyzing two laser thermal energy calculation equations: a comparison of beer-lambert's law and light transport equation, *Engineered Science*, 2023, **24**, 912, doi: 10.30919/es912.
[8] M. Harvey, W. L. Ong, M. Chao, C. Udovicich, S. McBride, D. Bolton, J. Eastham, M. Perera, Comprehensive review of the use of hydrogel spacers prior to radiation therapy for prostate cancer, *BJU International*, 2023, **131**, 280-287, doi: 10.1111/bju.15821.
[9] T. Narukawa, A. Fujihara, A. Ochiai, K. Okihara, F. Hongo, O. Ukimura, Role of hydrogel spacer to protect the rectum from thermal injury in focal therapy of prostate cancer: Preclinical study in cadaver model, *International Journal of Urology*, 2023, **30**, 116-118, doi: 10.1111/iju.15062.
[10] Q. Tang, F. Zhao, X. Yu, L. Wu, Z. Lu, S. Yan, The role of radioprotective spacers in clinical practice: a review, *Quantitative Imaging in Medicine and Surgery*, 2018, **8**, 514-524, doi: 10.21037/qims.2018.06.06.
[11] Z. Wang, S. Zhang, H. Wang, J. Huang, L. Wang, Effect of synergistic fermentation of Saccharomyces cerevisiae and Lactobacillus plantarum on thermal properties of hyaluronic acid-wheat starch system, *International Journal of Biological Macromolecules*, 2024, **267**, 131542, doi: 10.1016/j.ijbiomac.2024.131542.
[12] G. G. G. Perera, D. F. Argenta, T. Caon, The rheology of injectable hyaluronic acid hydrogels used as facial fillers: A review, *International Journal of Biological Macromolecules*, 2024, **268**, 131880, doi: 10.1016/j.ijbiomac.2024.131880.
[13] M. Afkhami Ardekani, H. Ghaffari, Optimization of prostate brachytherapy techniques with polyethylene glycol-based hydrogel spacers: A systematic review, *Brachytherapy*, 2020, **19**, 13-23, doi: 10.1016/j.brachy.2019.08.009.
[14] G. G. G. Perera, D. F. Argenta, T. Caon, The rheology of injectable hyaluronic acid hydrogels used as facial fillers: A review, *International Journal of Biological Macromolecules*, 2024, **268**, 131880, doi: 10.1016/j.ijbiomac.2024.131880.
[15] P. Namakshenas, A. Mojra, Optimization of polyethylene glycol-based hydrogel rectal spacer for focal laser ablation of prostate peripheral zone tumor, *Physica Medica*, 2021, **89**, 104-113, doi: 10.1016/j.ejmp.2021.07.034.
[16] P. J. Prada, J. Fernández, A. A. Martinez, Á. de la Rúa, J. M. Gonzalez, J. M. Fernandez, G. Juan, Transperineal injection of hyaluronic acid in anterior perirectal fat to decrease rectal toxicity from radiation delivered with intensity modulated brachytherapy or EBRT for prostate cancer patients, *International Journal of Radiation Oncology*Biology*Physics*, 2007, **69**, 95-102, doi: 10.1016/j.ijrobp.2007.02.034.
[17] X. Wu, K. Zhang, Y. Chen, R. Wang, L. Chen, A. Zhang, B. Hu, Theoretical and experimental study of dual-fiber laser ablation for prostate cancer, *PLoS One*, 2018, **13**, e0206065, doi: 10.1371/journal.pone.0206065.
[18] A. R. Bahramian, L. S. Ahmadi, M. Kokabi, Performance evaluation of polymer/clay nanocomposite thermal protection systems based on polyethylene glycol phase change material, *Iranian Polymer Journal*, 2014, **23**, 163-169, doi: 10.1007/s13726-013-0212-9.
[19] M. Bračič, S. Potrč, M. Finšgar, L. Gradišnik, U. Maver, H. Budasheva, D. Korte, M. Franko, L. Fras Zemljič, Amoxicillin doped hyaluronic acid/fucoidan multifunctional coatings for medical grade stainless steel orthopedic implants, *Applied Surface Science*, 2023, **611**, 155621, doi: 10.1016/j.apsusc.2022.155621.
[20] Z. Wang, S. Zhang, H. Wang, J. Huang, L. Wang, Effect of synergistic fermentation of Saccharomyces cerevisiae and Lactobacillus plantarum on thermal properties of hyaluronic acid-wheat starch system, *International Journal of Biological Macromolecules*, 2024, **267**, 131542, doi: 10.1016/j.ijbiomac.2024.131542.
[21] Y. Zhang, Generalized dual-phase lag bioheat equations based on nonequilibrium heat transfer in living biological tissues, *International Journal of Heat and Mass Transfer*, 2009, **52**, 4829-4834, doi: 10.1016/j.ijheatmasstransfer.2009.06.007.
[22] K.-C. Liu, Y.-S. Chen, Analysis of heat transfer and burn damage in a laser irradiated living tissue with the generalized dual-phase-lag model, *International Journal of Thermal Sciences*, 2016, **103**, 1-9, doi: 10.1016/j.ijthermalsci.2015.12.005.
[23] J. Hristov, Bio-heat models revisited: concepts, derivations, nondimensalization and fractionalization approaches, *Frontiers in Physics*, 2019, **7**, 189, doi: 10.3389/fphy.2019.00189.
[24] G. Zhang, M. Wang, F. Duan, K. Yuan, K. Li, J. Yan, Z. Chang, Y. Wang, Radiological findings of prostatic arterial anatomy for prostatic arterial embolization: preliminary study in 55 Chinese patients with benign prostatic hyperplasia, *PLoS One*, 2015, **10**, e0132678, doi: 10.1371/journal.pone.0132678.
[25] H. H. Pennes, Analysis of tissue and arterial blood temperatures in the resting human forearm, *Journal of Applied Physiology*, 1948, **1**, 93-122, doi: 10.1152/jappl.1948.1.2.93.
[26] Y. Ren, Y. Yan, H. Qi, Photothermal conversion and transfer in photothermal therapy: From macroscale to nanoscale, *Advances in Colloid and Interface Science*, 2022, **308**, 102753, doi: 10.1016/j.cis.2022.102753.
[27] M. Svatos, E. Chell, D. A. Low, V. Pigrish, P. F. Orio, K. Miller, M. T. King, Symmetry, separation, and stability: Physical properties for effective dosimetric space with a stabilized hyaluronic acid spacer, *Medical Physics*, 2024, **51**, 6231-6245, doi: 10.1002/mp.17292.
[28] J. Williams, K. M. Millan, D. Bolton, A. Tan, C. W. Cham, T. Pham, D. Pan, M. Liu, Y. Chan, P. Manohar, J. Thomas, G. Koufogiannis, H. Ho, M. Guerrieri, M. Ng, T. Boike, C. MacLeod, D. L. Joon, F. Foroudi, M. Chao, Hyaluronic acid rectal spacer in EBRT: usability, safety and symmetry related to user experience, *Journal of Medical Imaging and Radiation Sciences*, 2022, **53**, 640-647, doi: 10.1016/j.jmir.2022.09.008.
[29] G. Mok, E. Benz, J.-P. Vallee, R. Miralbell, T. Zilli,

Optimization of radiation therapy techniques for prostate cancer with prostate-rectum spacers: a systematic review, *International Journal of Radiation Oncology, Biology, Physics*, 2014, **90**, 278-288, doi: 10.1016/j.ijrobp.2014.06.044.
[30] P. Snetkov, K. Zakharova, S. Morozkina, R. Olekhnovich, M. Uspenskaya, Hyaluronic acid: the influence of molecular weight on structural, physical, physico-chemical, and degradable properties of biopolymer, *Polymers*, 2020, **12**, 1800, doi: 10.3390/polym12081800.

**Publisher's Note:** Engineered Science Publisher remains neutral with regard to jurisdictional claims in published maps and institutional affiliations.